Outgassing properties of additively manufactured aluminium

Ciarán Breen, James Walpole, Carolyn Atkins, Scott McPhee, Mark Cliffe, Jamie Moffat, Maisie Edwards-Mowforth, Isla Lister, Lucy Reynolds, Andrew Conley, Sam Allum, Robert M. Snell, Sam Tammas-Williams, Steve Watson

Outgassing properties of additively manufactured aluminium

Ciarán Breen[a], James Walpole[a], Carolyn Atkins[a], Scott McPhee[a], Mark Cliffe[a], Jamie Moffat[a], Maisie Edwards-Mowforth[a,b], Isla Lister[b], Lucy Reynolds[a,c], Andrew Conley[d], Sam Allum[e], Robert M. Snell[f], Sam Tammas-Williams[b], and Steve Watson[a*]

[a]UK Astronomy Technology Centre, Royal Observatory, Edinburgh, EH9 3HJ, UK
[b]School of Engineering, University of Edinburgh, Edinburgh, EH9 3FB, UK
[c]Dept of Physics, Durham University, Durham, DH1 3LE, UK
[d]Campus Technology Hub, Daresbury Laboratory, Keckwick Lane, Daresbury, WA4 4FS, UK
[e]Rutherford Appleton Laboratory, Harwell Campus, Didcot, OX11 0QX, UK
[f]Dept of Materials Science and Engineering, University of Sheffield, Sheffield, S1 3JD, UK

ABSTRACT

Details of a programme to investigate the outgassing rate of additively manufactured (AM) aluminium alloys are presented. AM has significant potential benefits to applications in ground- and space-based instrumentation, particularly in mass optimisation, part consolidation and increased design freedom. However, its use in high-risk projects is often curtailed by lack of heritage and an imperfect understanding of the materials. The programme goal was to address one of the most significant topics preventing wider adoption of AM technology in cryogenic and space-based applications; uncertainty about material outgassing. The sensitivity of outgassing rates to various key parameters was characterised, including print method, post-processing and geometrical complexity. Correlation of outgassing rates against other measurable properties, such as sample porosity and surface roughness, was also investigated via the use of X-ray computed tomography and profilometry. Finally, the test apparatus, experimental design and implications of the findings on design and process control are discussed.

Keywords: Additive manufacture, aluminium, porosity, outgassing, astronomical instrumentation, vacuum

1. INTRODUCTION

Additive manufacture (AM), commonly known as 3D printing, is a method of manufacture that builds a structure layer-by-layer from a digital design file. AM has several advantages over conventional manufacturing methods (subtractive, formative and fabricative), for example: it offers a much broader design space, allowing organic and lattice style structures to be incorporated; part consolidation, where multiple components can be created as one part reducing the need for fixtures; and reduced waste, as the near net shape is created. Astronomical telescopes and instrumentation for the research community are typically bespoke and one-offs. Therefore, the individual components that are used to make astronomical hardware have low part counts and often require geometrically complex designs to ensure that the hardware fits within the imposed volume and mass constraints. When considering the different methods of metal manufacture (cutting, casting, injection moulding), AM favours the case for low quantity and high geometric complexity parts.[1] Therefore, AM has clear benefits within the field of astronomical hardware.

There are several challenges associated with AM which currently contribute towards its lack of adoption within astronomical instrumentation,[2] for example: lack of standardisation, resulting in variable material properties; porosity, leading to potential areas of fracture and trapped gas; surface roughness, necessitating the need for machining interfaces and challenges in cleanliness; and, arguably, a lack of trained senior engineers able to implement AM successfully and to mentor early career engineers. However, none of these challenges are insurmountable. Standardisation is actively being defined within industry and academia, porosity can be minimised by optimising machine print parameters and thermal treatment, roughness can be reduced in post-processing

---

and there are numerous training courses now available for design for AM. The goal of this paper is to present a pilot study into one of the drawbacks resulting from AM porosity and surface roughness; an increase in the outgassing rate for instrumentation within a vacuum environment.

Vacuum and cryogenic environments are frequently required for astronomical hardware working in a range of wavelengths, for example infrared (IR) detectors are commonly cooled to ≤ 40 K within a cryostat, or, more generally, space-based astronomical observatories. Outgassing, where molecules are released from an object, is a common effect within a vacuum environment. It results in an increase in the base pressure achievable by the vacuum chamber and, potentially, in outgassed material plating on to cold surfaces in the system, causing detrimental thermal and optical effects. Understanding the magnitude of the outgassing rate for AM materials, and associated post-processing methods, will help designers utilise AM components within these environments.

Outgassing becomes the primary gas load on the system once the initial gas has been evacuated from the system and there are no process gas flows, leaks, or back-streaming from the pumps.[3] Contributions to outgassing come from vapourisation of the material, desorption of gas molecules that have adsorbed upon the surface, diffusion of molecules from within the material and permeation, where molecules have permeated from outside the vacuum through the material. Desorption of adsorbed molecules from the surface of a material is the primary reason why components undergo a rigorous cleaning and bakeout process prior to installation within a vacuum chamber. Furthermore, minimising microscopic surface area via good surface finishes reduces the likelihood of adsorption and, in turn, desorption. Therefore, ideal materials and structures for low outgassing are those that exhibit minimal surface area, good surface finish and are 100% dense and, as such, the outgassing rates of components made from bulk materials cannot be simply transferred to AM equivalents. In addition, one of the primary benefits of AM is the ability to reduce mass while maintaining structural performance by using lattice structures that are less easily post-processed and often have very high surface areas and raw, as-printed finishes - this combination is not ideal for low outgassing rates.

Outgassing rates within the literature for both bulk and AM materials are highly variable. The variation can be linked to the broad range of post-processing steps available to create a sample, and random and systematic errors which occur during this sensitive measurement. The outgassing behaviour of AM substrates remains a poorly studied characteristic.[4–7] This paper presents selected results of an initial study comparing the outgassing rate of bulk aluminium samples against as-printed and post-processed AM equivalents, and discusses planned future work. Section 2 presents the sample definition, outgassing method selection, calculation of the outgassing rate, the procedure followed and the accompanying internal and external metrology of the samples; Section 3 highlights the results from the study; and the summary and future work is described in Section 4.

2. METHOD

2.1 Samples

The long term study will eventually investigate a broad range of materials, including metals, polymers and composites, as well as different print processes. For each material, where possible, two geometries are printed; a cuboid box (termed 'cube' in this paper) and a lattice. The two geometries represent two different style geometries that could be used by AM in future astronomical hardware but they also represent two different types of print parameters (the AM machine parameters), as it is common for a different set of print parameters to be used for both lattices and solids. The sample geometries are shown in Figure 1, the bounding volume in each case is identical at 40 mm × 40 mm × 27.5 mm, whereas the surface areas, calculated within computer aided design (CAD) software, are 9708 mm² and 18 054 mm² for the cube and the lattice respectively. The wall and base thicknesses of the cube, as shown in Figure 1 *a)*, are 5.75 mm and 3.5 mm respectively. The lattice geometry is a body centred cubic with additional struts in the z-direction (BCCz), the BCC struts and the z struts are approximately 1.24 mm and 1.72 mm in diameter respectively. Both geometries were designed to ensure that support material was not required during the print process and so that equivalent bulk material cubes could be subtractively machined as references.

Table 1 displays the different materials, shapes, and print processes of samples that have been produced. For the aluminium and titanium samples, two different sets of AM machines were used: for aluminium, high spatial resolution and low spatial resolution laser powder bed fusion (L-PBF) prints were used, whereas the titanium
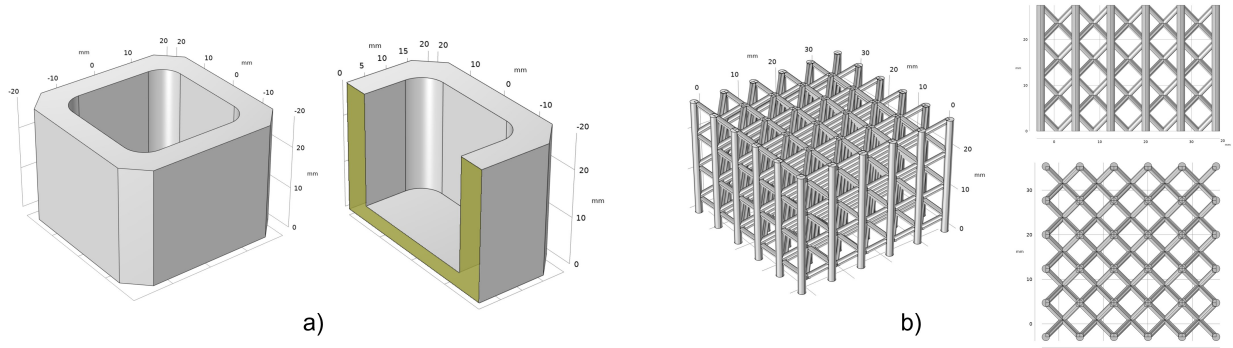
Figure 1: The sample geometries used within the study: *left a)* the 'cube' geometry and *right b)* the lattice geometry.

samples used a high resolution laser powder bed fusion print and an electron beam powder bed fusion (EB-PBF) print. The rationale behind the different print methods is the acknowledgement that two AM machines are likely to produce different quality AM substrates. In addition, for the AM cubes, two post-processing states were considered: raw, defined as no post-processing; and machined, where the external surfaces were machined using conventional techniques. Although machining the surfaces removes the as-printed roughness, there is a risk that it exposes internal porosity to the surface. However, ultimately, the inclusion of AM within astronomical hardware will require machining to create necessary interfaces and therefore is an important parameter in this study. For each sample variation, three samples were manufactured, therefore providing a total of $23 \times 3 = 69$ samples for the long term study. In the initial study, only the samples highlighted in blue text within Table 1 have been tested.

Material	Bulk	Additive manufacture		
Al 6082 T6	Cube	-	-	-
AlSi10Mg Low Res. (L-PBF)	-	Raw Cube	Machined Cube	Lattice
AlSi10Mg High Res. (L-PBF)	-	Raw Cube	Machined Cube	Lattice
Ti64	Cube	-	-	-
Ti64 (L-PBF)	-	Raw Cube	Machined Cube	Lattice
Ti64 (EB-PBF)	-	Raw Cube	Machined Cube	Lattice
ULTEM	-	Raw Cube	-	Lattice
Antero	-	Raw Cube	-	Lattice
Sicaprint	-	Raw Cube	-	Lattice

Table 1: A table of the sample variations tested. L-PBF=Laser Powder Bed Fusion and EB-PDF=Electron Beam Powder Bed Fusion

2.2 Outgassing Rate Measurement

2.2.1 Method Selection And Apparatus

The optimal experimental method is dependent on the magnitude of outgassing rates being measured since some techniques are only suitable for certain ranges of outgassing rates. It was considered very likely that the sample outgassing rates would vary by several orders of magnitude due to the different materials being used, particularly polymers, which generally have much higher outgassing rates than metals. This wide range combined with general uncertainty over expected outgassing rates of AM materials made it difficult to predict the range of outgassing rates that the experimental setup needed to measure. However, a lower bound was effectively set by the requirement to measure conventionally-manufactured metal samples, which have a very low outgassing rate requiring significant sensitivity.
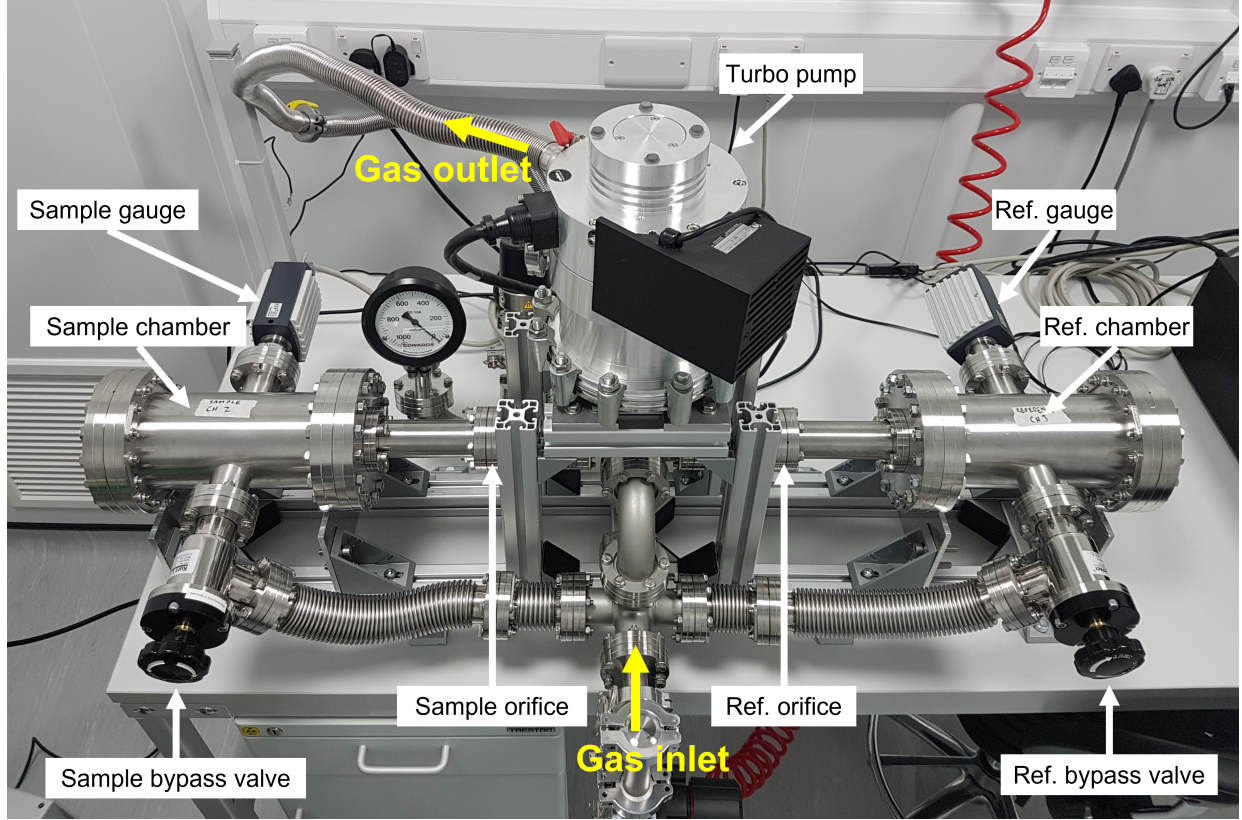
Figure 2: The outgassing rig with annotation, the rig is operated within a cleanroom environment to minimise ingress of contamination.

The detection of low outgassing rates required the background outgassing from the experimental setup to be removed effectively. For this reason, a difference method similar to that used by *Battes, et al. 2015*[8] and *Schindler, et al. 1996*[9] was selected. The difference method measures outgassing rates using a modified throughput method[10] where two almost identical chambers, one containing the sample and one empty, outgas through two small orifices into a pumped volume as shown in Figure 2. This allows the background outgassing rate to be measured simultaneously to the sample outgassing rate. The advantage of this method over running a blank test with the normal throughput method was that the effect of temperature fluctuations on the background outgassing rate is removed. The background rate could also fluctuate between tests and this method removes the need to take separate background measurements before every test.

The measured outgassing rate of the sample depends on the pressure of the chamber that the sample is placed in due to the effect of readsorption.[11] Therefore it was desired that all samples be subject to similar pressure conditions. Given the wide range of outgassing rates that were anticipated, sample outgassing would be the dominant gas source in the chamber and thus the pressure conditions could have varied by several orders of magnitude between the polymer and metal samples. The chamber pressure can be adjusted by changing the size of the orifice and thus pumping conductance. For this reason $0.75\,\text{mm}$, $1\,\text{mm}$, $5\,\text{mm}$ and $20\,\text{mm}$ orifices (with $1\,\text{mm}$ thickness) were created.

2.2.2 Calculation of the Outgassing Rate

The outgassing rate was calculated from:

$$q = \frac{C_S(p_S - p_{main}) - C_R(R(p_R) - p_{main})}{A} \quad \text{where} \quad R(p_R) = ap_R^3 + bp_R^2 + cp_R + d \tag{1}$$

where q is the outgassing rate, p is the pressure, C is the conductance, A is the surface area of the sample, and $R(p_R)$ quantifies any differences between the test and reference chambers. The subscripts S and R refer to the sample and reference chambers in Figure 2. The *main* subscript refers to the pressure within the central cross between the two orifices. C refers to the conductances of path from the sample and reference chambers to the main chamber. The factors a, b, c, and d are determined by a blank measurement. A blank measurement has $q = 0$ so rearranging Equation 1 gives:

$$ ap_R^3 + bp_R^2 + cp_R + d = \frac{C_S}{C_R} p_{T,blank} + \left(1 - \frac{C_S}{C_R}\right) p_{main} \tag{2} $$

A least squares fit to the chamber pressures from the blank measurement gives values of a, b, c, and d. Given the similarity between the chambers it was expected that $R(p_R)$ would be very close to a linear function of p_R.

C_S and C_R did not need to be equal but the values would ideally be close to each other to ensure that both chambers are as similar as possible. For simplicity, they were kept equal for this test so that the main chamber pressure terms cancelled out in Equation 1. The conductance of a circular aperture, C_a in a vacuum system is determined by:

$$ C_a = A_a \sqrt{\frac{RT}{2\pi M_m}} \simeq 11.6 A_a \tag{3} $$

where A_a is the cross-sectional area of the aperture, T is the temperature, and M_m is the mean molecular mass of the gas passing through the aperture.[12] The approximation is for air at 293 K where C is in l s^{-1} and A is in cm^2. This approximation is used to calculate the outgassing rates presented in this paper. The planned inclusion of a Residual Gas Analyzer (RGA) and temperature probes will allow for the direct measurement of M_m and T respectively.

Equation 3 assumes molecular flow conditions which occur when the mean free path is much greater than the diameter of the conducting vessel. This applies when $Pd \ll 0.1$ where P is the pressure in mbar and d is the diameter of the conducting vessel in mm.[12] Since for these outgassing tests $d = 0.75$ mm, molecular flow conditions apply at $P \leq 1 \times 10^{-2}$ mbar $\equiv 1$ Pa.

Equation 3 is true for an circular aperture where the thickness of the plate is much smaller than the diameter of the orifice. For tubes where the length is of the same order of magnitude or larger than the diameter, the transmission probability, α, must also be taken into account as a multiplying factor in Equation 3.[12] This can be estimated from:

$$ \alpha = \frac{1}{1 + \frac{3}{8}\frac{l_e}{R}} \quad \text{where} \quad \frac{l_e}{l} = 1 + \frac{1}{3 + \frac{3}{7}\frac{l}{R}} \tag{4} $$

where l is the thickness of the orifice plate, R is the radius of the orifice, and l_e is the equivalent length.[12] Equation 3 then becomes:

$$ C_a = \alpha A_a \sqrt{\frac{RT}{2\pi M_m}} \simeq 11.6 \alpha A_a \tag{5} $$

2.2.3 Cleaning Process

The samples were all cleaned before testing according to the following procedure:[13]

1. The samples were cleaned in an ultrasonic tank with a small concentration of detergent for 15 minutes at 50 °C.

2. They were then rinsed with tap water.

3. Excess water was removed with an air gun.

4. The samples were then placed in an aluminium foil tray and dried in an oven at 100 °C for 2 hours.

The drying process was not intended to fully bake the samples but to ensure that the majority of moisture introduced during cleaning was removed.
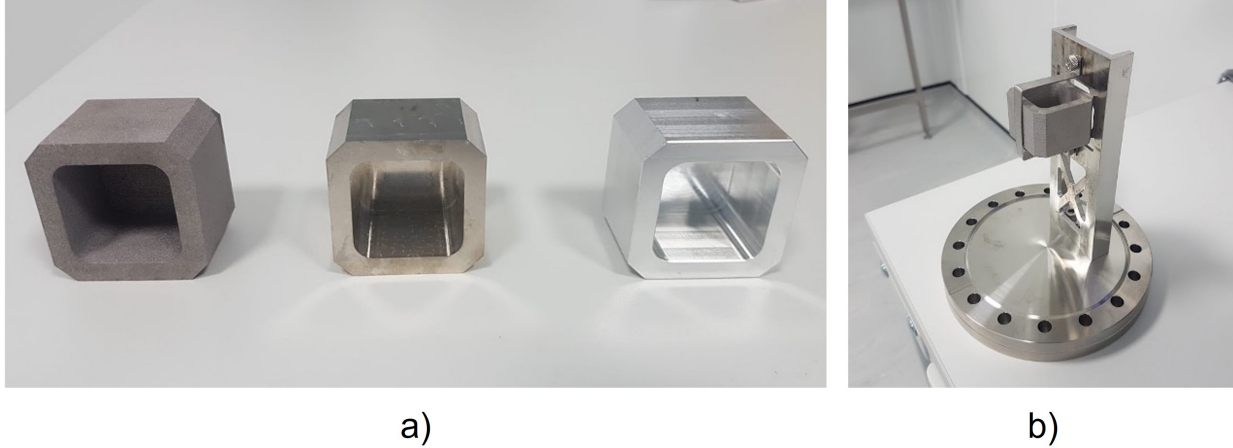
Figure 3: The samples used within the initial study: *a) left to right* Al high res. raw cube, Al high res. machined cube, and Al bulk machined cube; and *b)* a sample situated within its cradle, which is attached to a CF flange.

2.2.4 Test procedure

Starting with a system at vacuum, the chambers were backfilled with dry nitrogen to ~1000 mbar, then equalised to atmospheric pressure. The nitrogen occupies sites on the surface of the chambers where water would otherwise adsorb, which results in lower background water outgassing in the chambers. Once the system was at atmosphere, the chambers were opened and the sample was placed in the sample chamber holder, as shown in Figure 3. The reference chamber contained a piece of aluminium with a similar surface area to the sample holder. This ensured that the outgassing from the holder is accounted for in the background subtraction and does not contribute to the sample outgassing rate.

Each outgassing test lasted for at least 10 hours at room temperature. Initially the orifice bypass valves were open to quickly bring the chambers down to baseline pressure. The orifice bypass valve was closed once the reference chamber pressure dropped below 5.5×10^{-5} mbar so that for each test the chambers had a similar amount of material removed when the test began, regardless of the orifice size used. This value was chosen to keep the pressures within the range of a single filament current setting of the cold-cathode ion gauges over the full test period - automatic current switching introduces a perturbation to the measured pressure and confuses the signal. Measurements began when the bypass valves were closed. During the test the pressures in the test chamber and reference chamber were recorded. 10 hours was selected as the minimum duration of test as this compares to common values in the literature. An example of a test measurement using an AM sample is shown in Figure 4.

Between each group of samples a reference measurement of at least 10 hours was completed to allow $R(p_R)$ to be determined - an example is shown in Figure 5. The coefficients a, b, c, and d of $R(p_R)$ were calculated by applying a least squares fit to Equation 2. Since a blank measurement was taken before and after each group of samples, the blank measurement used to calculate $R(p_R)$ for each individual test was determined by which one was closest in time to the start of the test.

The surface areas of the samples were found from the CAD files used to produce them. This allowed for the calculation of the outgassing rate per unit surface area. These surface areas were not perfectly accurate even without accounting for the effect of microscopic surface roughness on surface area; this is especially true for the AM samples where geometrical tolerances are looser. The conductances C_S and C_R were calculated according to Equation 3 using the approximation is for air at 293 K. The outgassing rate for each sample was then determined as a function of time using Equation 1 and the $R(p_R)$ function calculated from the blank test.

2.3 Internal metrology: X-ray computed tomography

To assess to magnitude of porosity within the AM structures X-ray computed tomography (XCT) was used to assess the internal material structure. In the initial study only the aluminium lattices, both high and low
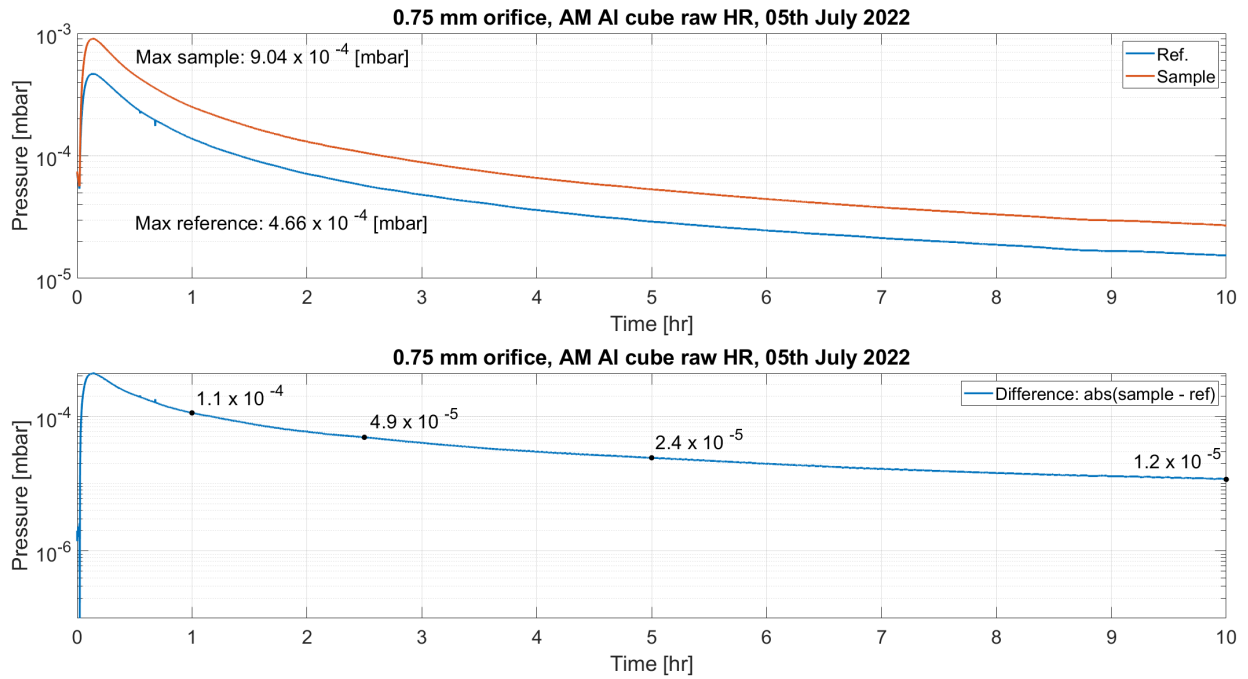
Figure 4: An example of a raw AM aluminium cube pressure measurement (*upper*) and the absolute difference between the sample and reference chamber pressures (*lower*).
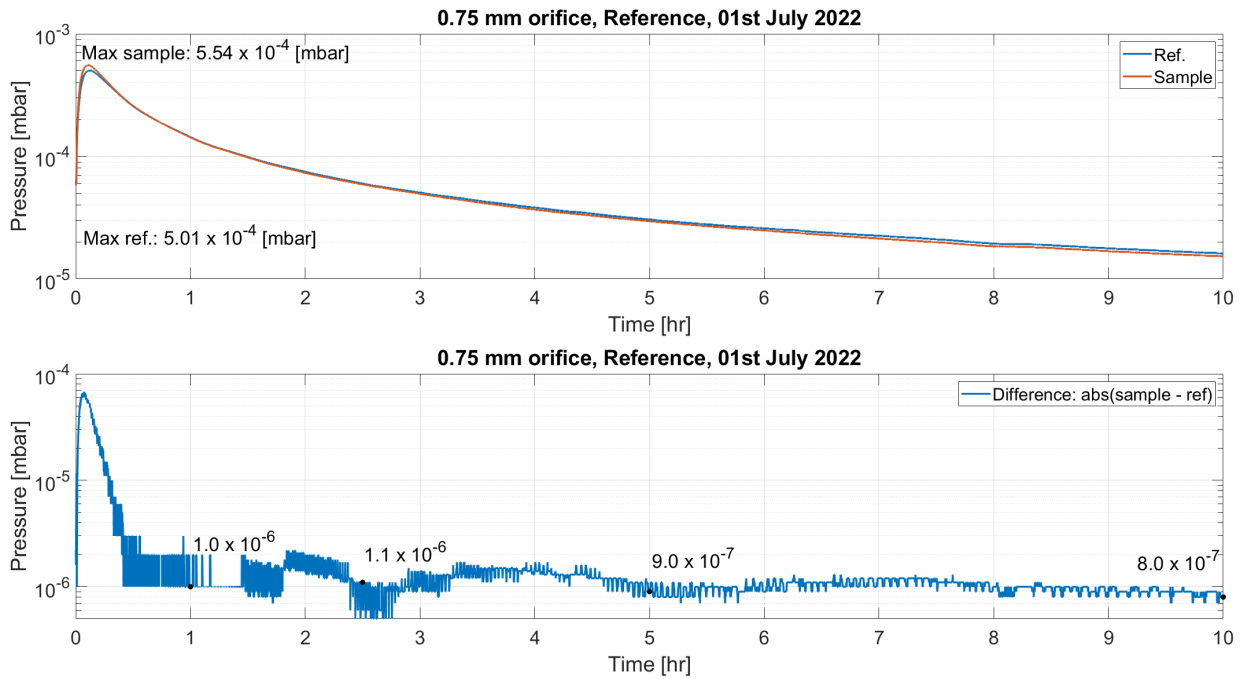

Figure 5: An example of a reference pressure measurement (*upper*) and the absolute difference between the sample and reference chamber pressures (*lower*).
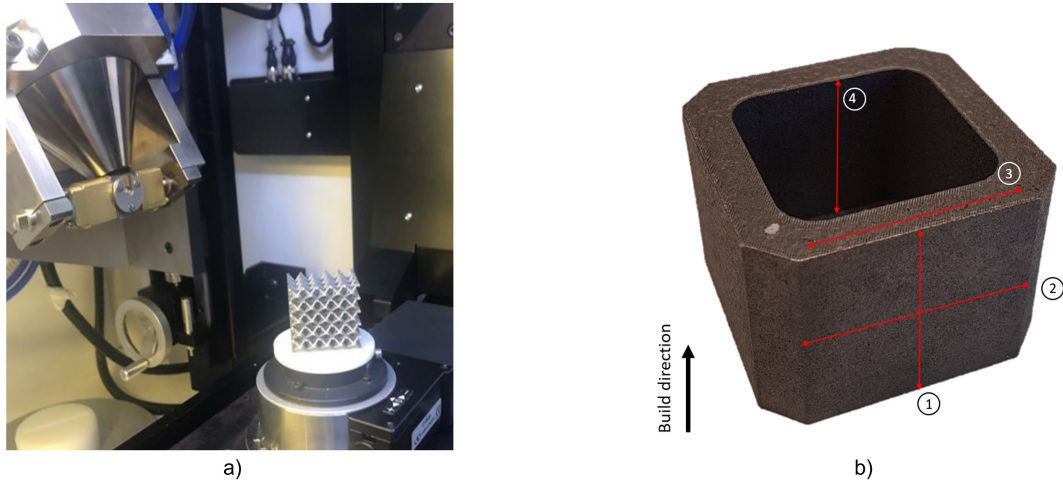
Figure 6: Internal and external metrology of the AM samples: *left a)*, an AM Al lattice sample within the XCT (image credit: W. Sun, NPL); and *right b)* the external profiles measured by the contact profilometer on each of the cube faces.

resolution, were evaluated. The aluminium samples were measured at $130\,\text{kV}$ and $60\,\mu\text{A}$, the voxel resolution achieved was $28\,\mu\text{m}$. Figure 6 *a)* highlights one of the lattice samples within the XCT. The XCT measurement data was exported as a series of ∼1450 image slices, RGB TIFF files, where the space between slices was the voxel resolution. An initial qualitative analysis of the XCT data was conducted within Matlab, a further more quantitative analysis was undertaken using commercial 3D data analysis software.

2.3.1 2D Analysis

An initial 2D analysis was undertaken within Matlab to qualitatively identify porosity within the samples. First, an RGB TIFF image was converted into a greyscale, where each pixel represented an intensity value. The pixels representing the lattice in the greyscale image were identified using the Otsu method,[14] which applied a threshold value to identify the lattice from the background. A binary image was created from the threshold output which identified the lattice as true (1) and the background as false (0). At this stage, 'porosity' within the lattice was identified as false, therefore to include the internal lattice voids as part of the sample (1), as opposed to the background (0), erosion and dilation operations were performed. From these steps the lattice, plus internal voids, could be extracted from the image file.

The identification of porosity within the lattice used edge detection, with a Sobel operator,[15] on the extracted greyscale image of the lattice. At this stage there was a manual alteration of the edge detection threshold so that the identified pores were accurately represented the pores that were identified by eye - quantification of porosity within XCT data is a challenging field and often subject to user interpretation. The identified pores were then subject to four criteria that removed pores if they were located too close to the edge, if they were less than 2 pixels and if they did not appear darker than the neighbouring pixels.

2.3.2 3D Analysis

Commercial 3D analysis software was used to investigate the 3D relationship of porosity within the low resolution and high resolution lattice samples. The individual TIFF images were loaded within the software and converted into a 3D dataset. The lattice was extracted using a threshold value calculated using the Otsu method and the external surface skin was removed to ensure only pores internal to the lattice were considered. A distance map was created by considering the minimum distance to the surface for each voxel within the lattice and this was then linked to the identified pores. The volume and distance information relating to each pore was then imported within Matlab for further analysis.
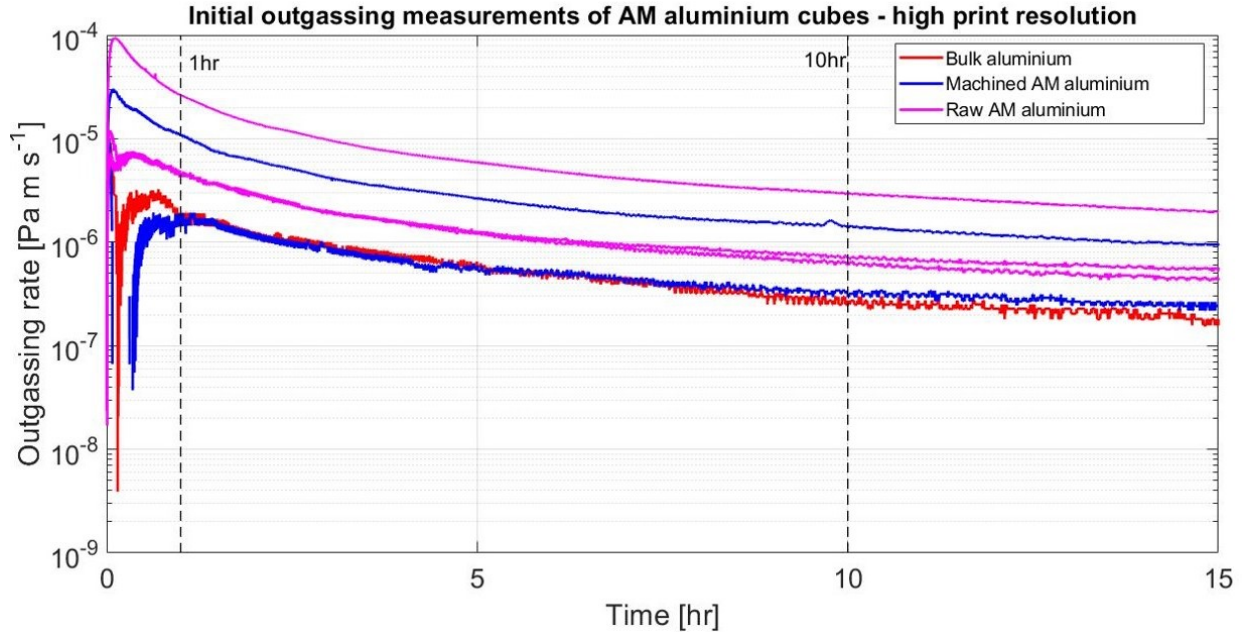
Figure 7: The outgassing rate as a function of time for bulk aluminium, machined AM HR aluminium and raw AM HR aluminium.

2.4 External metrology: Roughness measurements

The surface roughness of the cube samples was measured using a Form Talysurf Intra Touch contact profilometer with a diamond tip stylus. For every cube each face was measured as described in Figure 6 b), which led to 16 measurements per cube - the average of these measurements would describe the roughness of the sample. Measuring different orientations allowed the the roughness in the build direction and at 90° to the build direction to be sampled.

2.4.1 Analysis

The individual profiles were analysed within Matlab to determine the roughness parameters: R_a (mean), R_q (root mean square), R_t (peak to valley over evaluation length) and R_z (peak to valley over sampling length). The evaluation length (L_e) is defined as the total measurement length ($\sim$25 mm) and the sampling length (L_s) is defined by the filter cut off (λ_c), which is used to remove the form and waviness of the profile so that only the roughness within the profile remains. A λ_c value is defined by the anticipated roughness R_a of the part, following the ISO 4288-1996 standard, for R_a values between 0.1 µm $\rightarrow$ 2 µm and between 2 µm $\rightarrow$ 10 µm, λ_c values of 0.8 mm and 2.5 mm are required respectively - the roughness of the machined and raw cubes were expected within these values. Therefore, the sampling lengths of the R values are equivalent to the λ_c values - example, assuming a 25 mm evaluation length, there will be 10 individual roughness measurements for a λ_c = 2.5 mm (L_e/λ_c = 25/2.5 = 10 roughness measurements). Therefore, the roughness values quoted reflect the average of the maximum number of sampling lengths that can be accommodated within the evaluation length.

3. RESULTS

3.1 Outgassing Rates

Figure 7 and Table 2 present the outgassing rates in $\mathrm{Pa\,m\,s^{-1}}$ over a 15 hour period. In this initial study only the following samples were studied: one bulk Al cube, three AM raw cube Al HR, and two AM mach cube Al HR. As seen, there is an approximate order of magnitude (factor of 10) difference within the measured data for the same sample type and therefore implies some discrepancies in either the cleaning process, the homogeneity between AM samples, or measurement process.

Sample	Outgassing rate [Pa m s^{-1}]	
	1 hr	10 hrs
Bulk cube 6082 T6	1.9×10^{-6}	2.5×10^{-7}
AM raw cube AlSi10Mg high res. #1	4.7×10^{-6}	6.0×10^{-7}
AM raw cube AlSi10Mg high res. #2	2.6×10^{-5}	2.9×10^{-6}
AM raw cube AlSi10Mg high res. #3	4.6×10^{-6}	7.0×10^{-7}
AM mach. cube AlSi10Mg high res. #1	1.1×10^{-5}	1.4×10^{-6}
AM mach. cube AlSi10Mg high res. #2	1.4×10^{-6}	3.2×10^{-7}

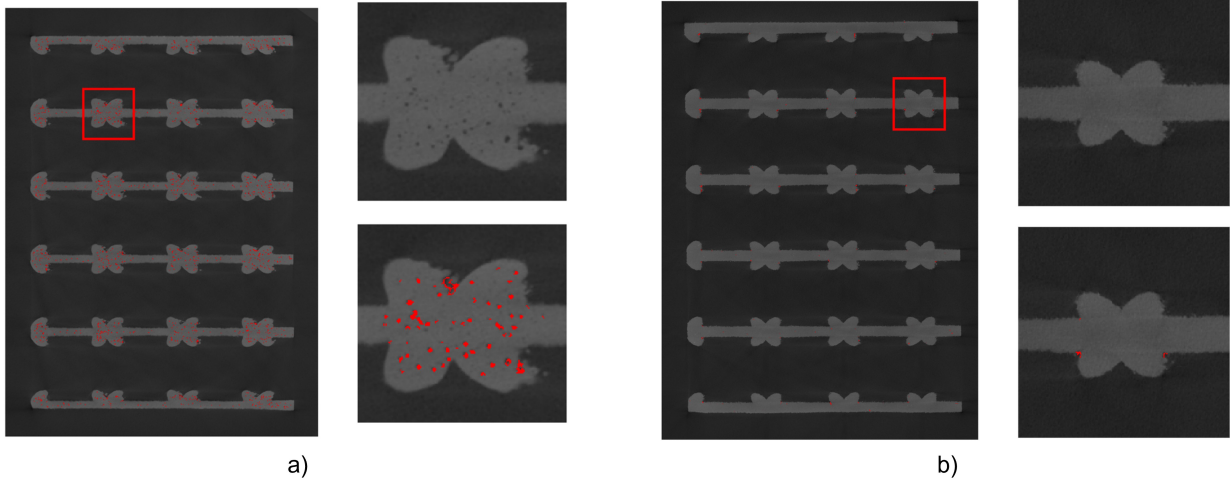Table 2: The outgassing rates at 1 hr and at 10 hrs.

Figure 8: Initial 2D XCT analysis of the lattice: *left a)* highlights the low resolution aluminium print; and *right b)* highlights the high resolution print. The regions shaded in red refer to the porosity identified within the sample.

3.2 XCT 2D porosity analysis

An extract of the 2D results from the XCT is presented in Figure 8. Although a quantitative analysis in this case was not performed, qualitatively, the low resolution aluminium prints have significantly more porosity than the high resolution prints.

3.3 XCT 3D porosity analysis

Figure 9 presents a quantitative 3D analysis of a high resolution and a low resolution aluminium lattice. The histogram describes the distribution of individual pores relative to shortest distance to the surface. The plots demonstrate quantitatively the increase in porosity of the low resolution lattice compared to the high resolution lattice, but also that the low resolution porosity is more likely to occur between 0.30 mm to 0.43 mm from the surface, whereas the high resolution lattice porosity is dominantly located near the edge of the lattice, between 0.03 mm to 0.10 mm. However, it should be noted that the maximum of the high resolution histogram, ~ 300 pores, is less than the equivalent location in the low resolution print at ~ 3000 pores.

Figure 10 presents a planar view of the 3D analysis for the two lattice types. The increase in porosity for the low resolution lattice is clearly shown and agrees with the 2D analysis. Furthermore, the increase in roughness on the down-surface of the struts, that is the bottom surface of the strut relative to the build plate, is clearly shown in the low resolution lattice, in contrast the same effect in the high resolution lattice is less pronounced.

Considering both the 2D and 3D XCT analysis the expectation is that the low resolution lattice will outgas more than the high resolution lattice based upon the increase in porosity and the increased roughness on the down-surface of the BCC lattice. However, given that diffusion is likely to be the dominant mechanism for gas
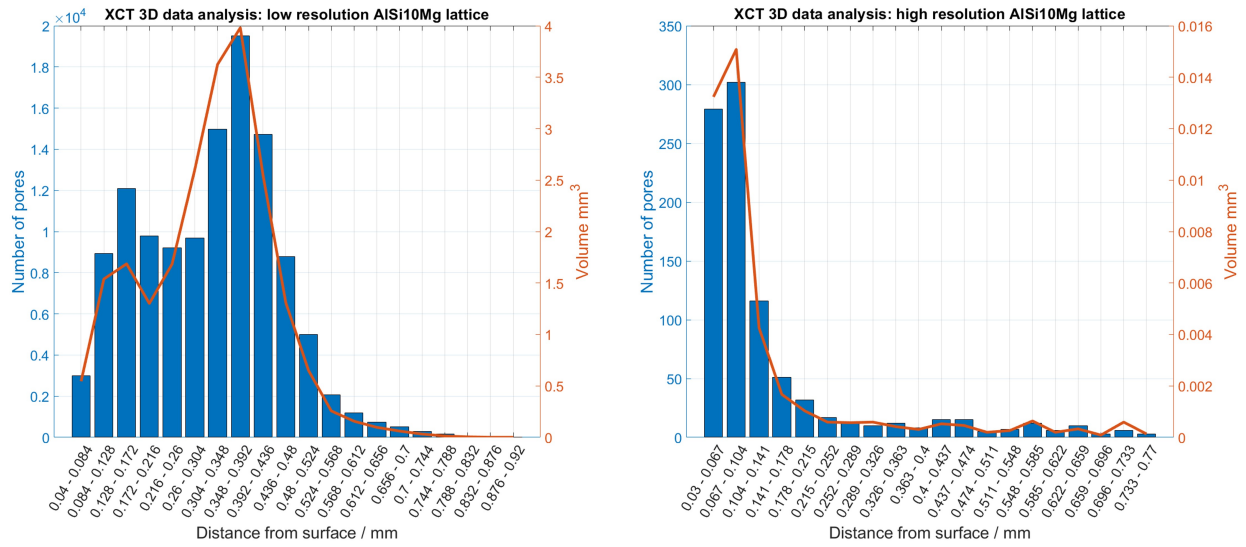
Figure 9: Examples of the distribution of individual pores relative to shortest distance to the surface: *left* - low resolution AlSi10Mg, and *right* - high resolution AlSi10Mg.
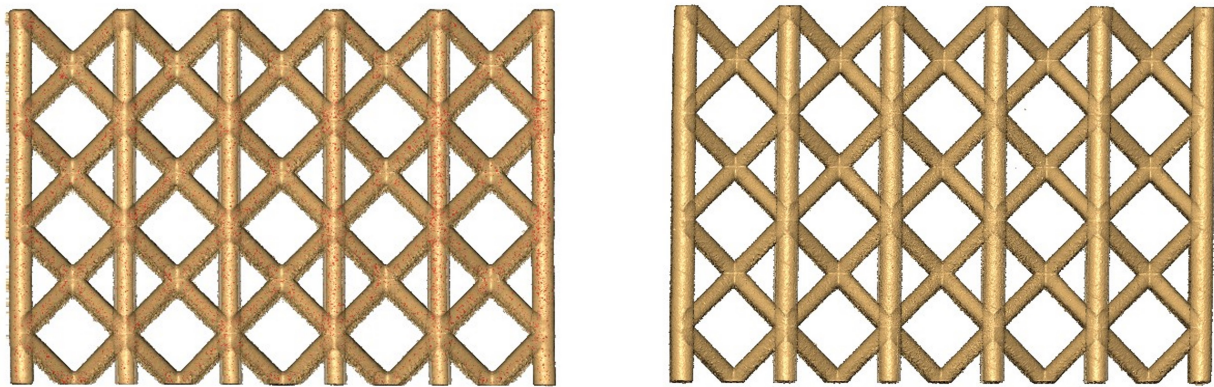

Figure 10: A planar view of the 3D analysis, low resolution *left* high resolution *right*, where the external surface is transparent and the pores are highlighted in red, therefore the pores are cumulative normal to the plane.

Cube sample	$\lambda_c = 0.8\,\mathrm{mm}$ / R [µm]				$\lambda_c = 2.5\,\mathrm{mm}$ / R [µm]			
	R_a	R_q	R_t	R_z	R_a	R_q	R_t	R_z
AM AlSi10Mg raw HR	9.65	12.15	91.96	3.12	11.30	14.60	106.00	75.20
AM AlSi10Mg raw LR	5.61	7.30	66.33	3.21	8.51	11.00	82.80	54.30
AM Ti64 raw HR	9.43	11.67	77.32	3.05	17.30	21.20	126.00	90.60
AM Sicaprint	7.16	8.94	65.68	4.92	8.47	10.70	72.50	55.80
AM AlSi10Mg mach. HR	0.17	0.24	5.21	0.13	0.23	0.31	4.94	0.22
AM AlSi10Mg mach. LR	0.16	0.23	5.06	0.13	0.21	0.30	5.08	0.29
Bulk mach. 6082 T6	0.22	0.28	2.90	0.07	0.27	0.35	3.03	0.09

Table 3: Surface roughness parameters measured for each material studied within the project. Parameters are calculated on a filtered surface profile with λ_c values of 0.8 mm and 2.5 mm

molecules to eventually desorb, it might be that this effect is more significant at a longer test duration (>20 hours). Although it is suspected that the porosity seen in the lattices would replicate in the cubes, this has yet to be investigated.

3.4 Surface Roughness

Table 3 presents the collation of the four calculated roughness values using λ_c at 0.8 mm and 2.5 mm for the cube samples in the different materials and post-processing methods. The roughness values for the machined samples are, as expected, the lowest within the set given the profilometer is measuring the tool marks used in machining. The high resolution prints in both aluminium and titanium exhibit the highest degree of roughness at ~12 µm R_q at $\lambda_{0.8}$ and a more significant difference at $\lambda_{2.5}$ where titanium exhibits ~21 µm and aluminium ~15 µm R_q. The difference observed at $\lambda_{2.5}$ implies the presence of a waviness with a period between 0.8 mm and 2.5 mm.

The effect of surface roughness on outgassing rates would imply that the high resolution raw cubes have surfaces that are more likely to adsorb and desorb molecules than low resolution or machined cubes. Although the outgassing rates presented in Figure 7 represent an initial study, it is observed that the raw aluminium high resolution cubes have a high outgassing rate than the machined counterparts.

3.5 Discussion

The initial results highlight discrepancies within outgassing rates for near-identical samples, which require further investigation to understand their origins. For example, the sensitivity of outgassing rate to location on the AM build plate will be investigated. However, the outgassing rates generally agree with the predicted trend that the rougher samples exhibit higher outgassing rate.

Throughout the initial test programme, a number of errors were identified and addressed, such as backstreaming from a leaking relief valve, current switching in the pressure gauges and inconsistent cleaning and test procedures. An upgrade to the outgassing rig is planned in the near term to remove some of the errors associated with the accuracy of the 0.75 mm orifice plate and to install an appropriately pressure rated valve to isolate the gas inlet from the main chamber. Repeatability tests will be conducted to verify the ability of the apparatus to provide reliable results.

4. SUMMARY AND FUTURE WORK

The goal of this paper was to present the results from an initial study into the outgassing rates of AM aluminium components and to introduce the community to the planned larger study into a broader range of material and sample geometries. To achieve this goal, the sample range, methodology, accompanying metrology, and analysis, have been presented. The initial outgassing rates indicate a high degree of variability within samples of the same material and post-processing method and we aim to reduce this variability in the immediate future through an improved procedure, new components, and a repeatability study. Despite the variability, the samples measured follow the expected trend in outgassing when considering the roughness of each surface.

Following the immediate second iteration of the initial study, future work will bring online further instrumentation to support the measurements, such as temperature sensors connected to the rig; a residual gas analyser to monitor the chemical species desorbed; and corroboration of the outgassing rates through external mass loss measurements. Following the upgrade and with increased confidence in the rig's performance, all materials, post-processing methods and geometries described in Table 1 will be tested. The results of the study will be made open access for the community following completion. Following completion of this study, the rig will be used to explore further AM materials of interest as well as specific AM geometries developed in-house, as part of the on-going AM astronomical hardware development programme.

5. ACKNOWLEDGEMENTS

REFERENCES

[1] Levy, G. N., Schindel, R., and Kruth, J., "Rapid manufacturing and rapid tooling with layer manufacturing (LM) technologies, state of the art and future perspectives," *CIRP Annals* **52**(2), 589–609 (2003).

[2] Atkins, C., van de Vorst, L. T. G. B., Farkas, S., Hugot, E., Mező, G., Morris, K., Roulet, M., Snell, R., , Sanginés, F. T., Todd, I., Vega-Moreno, A., and Schnetler, H., "The OPTICON A2IM Cookbook: an introduction to additive manufacture for astronomy," **12188-29**, International Society for Optics and Photonics, SPIE (2022).

[3] Grinham, R. and Chew, A., "A Review of Outgassing and Methods for its Reduction," *Appl. Sci. Converg. Technol.* **26**, 95–109 (Sept. 2017).

[4] Povilus, A. P., Wurden, C. J., Vendeiro, Z., Baquero-Ruiz, M., and Fajans, J., "Vacuum compatibility of 3D-printed materials," *Journal of Vacuum Science & Technology A: Vacuum, Surfaces, and Films* **32**, 033001 (May 2014).

[5] Pastore, R., Delfini, A., Albano, M., Vricella, A., Marchetti, M., Santoni, F., and Piergentili, F., "Outgassing effect in polymeric composites exposed to space environment thermal-vacuum conditions," *Acta Astronautica* **170**, 466–471 (May 2020).

[6] Gans, A. R., Jobbins, M. M., Lee, D. Y., and Alex Kandel, S., "Vacuum compatibility of silver and titanium parts made using three-dimensional printing," *Journal of Vacuum Science & Technology A: Vacuum, Surfaces, and Films* **32**, 023201 (Mar. 2014).

[7] Bihari, N., Heikkinen, I. T. S., Marin, G., Ekstrum, C., Mayville, P. J., Oberloier, S., Savin, H., Karppinen, M., and Pearce, J. M., "Vacuum outgassing characteristics of unpigmented 3D printed polymers coated with atomic layer deposited alumina," *Journal of Vacuum Science & Technology A* **38**, 053204 (Sept. 2020).

[8] Battes, K., Day, C., and Hauer, V., "Outgassing rate measurements of stainless steel and polymers using the difference method," *Journal of Vacuum Science & Technology A: Vacuum, Surfaces, and Films* **33**, 021603 (Mar. 2015).

[9] Schindler, N., Schleubner, D., and Edelmann, C., "Measurements of partial outgassing rates," *Vacuum* **47**, 351–355 (Apr. 1996).

[10] Redhead, P. A., "Recommended practices for measuring and reporting outgassing data," *Journal of Vacuum Science & Technology A: Vacuum, Surfaces, and Films* **20**, 1667–1675 (Sept. 2002).

[11] Redhead, P. A., "Effects of readsorption on outgassing rate measurements," *J. Vac. Sci. Technol. A* **14**(4), 12 (1996).

[12] Lafferty, J. M., ed., [*Foundations of vacuum science and technology*], Wiley, New York (1998).

[13] Chambers, A., [*Modern Vacuum Physics*], CRC Press (Aug. 2004). Google-Books-ID: AnvMBQAAQBAJ.

[14] Bangare, S. L., Dubal, A., Bangare, P. S., and Patil, S., "Reviewing Otsu's Method For Image Thresholding," *International Journal of Applied Engineering Research* **10**, 21777–21783 (May 2015).

[15] Zhang Jin-Yu, Chen Yan, and Huang Xian-Xiang, "Edge detection of images based on improved Sobel operator and genetic algorithms," in [*2009 International Conference on Image Analysis and Signal Processing*], 31–35, IEEE, Linhai, China (2009).